



Review

Electrochemical Synthesis of Ammonia via Nitrogen Reduction and Oxygen Evolution Reactions—A Comprehensive Review on Electrolyte-Supported Cells

Hizkia Manuel Vieri ¹ , Moo-Chang Kim ^{1,2}, Arash Badakhsh ³  and Sun Hee Choi ^{1,4,*}

¹ Hydrogen-Fuel Cell Research Center, Korea Institute of Science and Technology (KIST), Seoul 02792, Republic of Korea; hizkiamanuelvg@kist.re.kr (H.M.V.); k123w03@seoultech.ac.kr (M.-C.K.)

² Department of Mechanical and Automotive Engineering, Seoul National University of Science and Technology, Seoul 01811, Republic of Korea

³ PNDC, University of Strathclyde, Glasgow G68 0EF, UK; arash.badakhsh@strath.ac.uk

⁴ Energy & Environment Technology, KIST School, University of Science and Technology (UST), Seoul 02792, Republic of Korea

* Correspondence: shchoi@kist.re.kr; Tel.: +82-10-9256-5908

Abstract: The application of protonic ceramic electrolysis cells (PCECs) for ammonia (NH₃) synthesis has been evaluated over the past 14 years. While nitrogen (N₂) is the conventional fuel on the cathode side, various fuels such as methane (CH₄), hydrogen (H₂), and steam (H₂O) have been investigated for the oxygen evolution reaction (OER) on the anode side. Because H₂ is predominantly produced through CO₂-emitting methane reforming, H₂O has been the conventional carbon-free option thus far. Although the potential of utilizing H₂O and N₂ as fuels is considerable, studies exploring this specific combination remain limited. PCEC fabrication technologies are being developed extensively, thus necessitating a comprehensive review. Several strategies for electrode fabrication, deposition, and electrolyte design are discussed herein. The progress in electrode development for PCECs has also been delineated. Finally, the existing challenges and prospective outlook of PCEC for NH₃ synthesis are analyzed and discussed. The most significant finding is the lack of past research involving PCEC with H₂O and N₂ as fuel configurations and the diversity of nitrogen reduction reaction catalysts. This review indicates that the maximum NH₃ synthesis rate is $14 \times 10^{-9} \text{ mol cm}^{-2} \text{ s}^{-1}$, and the maximum current density for the OER catalyst is 1.241 A cm^{-2} . Moreover, the pellet electrolyte thickness must be maintained at approximately 0.8–1.5 mm, and the stability of thin-film electrolytes must be improved.

Keywords: electrochemical ammonia synthesis; protonic ceramic electrolysis cells; hydrogen; catalysts; nitrogen reduction reaction



Citation: Vieri, H.M.; Kim, M.-C.; Badakhsh, A.; Choi, S.H. Electrochemical Synthesis of Ammonia via Nitrogen Reduction and Oxygen Evolution Reactions—A Comprehensive Review on Electrolyte-Supported Cells. *Energies* **2024**, *17*, 441. <https://doi.org/10.3390/en17020441>

Academic Editor: Antonino S. Arico

Received: 8 December 2023

Revised: 5 January 2024

Accepted: 14 January 2024

Published: 16 January 2024



Copyright: © 2024 by the authors. Licensee MDPI, Basel, Switzerland. This article is an open access article distributed under the terms and conditions of the Creative Commons Attribution (CC BY) license (<https://creativecommons.org/licenses/by/4.0/>).

1. Introduction

Hydrogen (H₂) has considerable potential for energy storage. However, its low energy density poses challenges to storage and transport. One solution is to convert H₂ to ammonia (NH₃), where H₂ that is obtained from water electrolysis (i.e., green H₂) reacts with nitrogen (N₂) in the air to produce NH₃, which can be reversibly converted into H₂ and N₂ after transportation [1]. Currently, NH₃ is industrially produced using the Haber–Bosch process, which requires high pressure (100–200 bar) and temperature (300–400 °C) to activate the Fe-based catalysts [2,3]. Recent advancements include the hydrogenation of N₂ using Ru catalysts, which require milder reaction conditions [4].

However, the thermal approach for NH₃ synthesis remains expensive, as it requires a large centralized infrastructure and is energy-intensive, consuming approximately 485 kJ mol⁻¹ (approximately 2% of the global energy use per annum) [5]. Fertilizers Europe made conjectures about the decarbonization of the European NH₃ industry [6].

They proposed that approximately 10% of H_2 derived for NH_3 production in 2030 could possibly originate from renewable sources. Electrochemical NH_3 synthesis via N_2 reduction provides a relatively high efficiency of up to 20%, environmental compatibility with renewable sources (solar, tidal, and wind), on-site H^+ generation from water oxidation, and adaptable reaction control [7]. This process converts sustainable electricity from sources such as wind power into NH_3 for use as a synthetic fuel or chemical feedstock [8,9].

The operating conditions are classified into three types based on the temperature, namely, low ($<100\text{ }^\circ\text{C}$), intermediate ($200\text{--}500\text{ }^\circ\text{C}$), and high ($>400\text{ }^\circ\text{C}$) temperature. High-temperature conditions enhance the catalytic activity and substantially increase the Faradaic efficiency in NH_3 synthesis. High-temperature NH_3 synthesis can be performed using proton-conducting electrolytes (PCEs) or oxygen-conducting electrolytes (OCEs). OCEs, while efficient, generally present slower rates of NH_3 production than PCEs [10]. This review focuses on NH_3 production in protonic ceramic electrolysis cells (PCECs), which operate at high temperatures ($400\text{--}600\text{ }^\circ\text{C}$). As shown in Figure 1, the PCEC combines the nitrogen reduction reaction (NRR) with other electrochemical reactions that yield protons (H^+), facilitating NH_3 production. Liu et al. briefly reviewed three primary PCEC configurations involving H_2 , CH_4 , and H_2O as proton (H^+) sources. Although H_2O and N_2 have considerable potential as fuels, this specific combination has not been sufficiently investigated. Despite consuming substantially more electrical energy than the other configurations, using H_2O and N_2 directly to produce NH_3 is carbon-free and abundant in the feedstock [11]. This configuration couples the NRR with the oxygen evolution reaction (OER). High-temperature NH_3 synthesis has been extensively reviewed [12–16]. However, reviews of the specific PCEC configurations for NH_3 synthesis are limited. The unavailability of a comprehensive strategy for PCEC fabrication in a single study poses a considerable challenge for researchers aiming to develop PCECs customized for NH_3 synthesis.

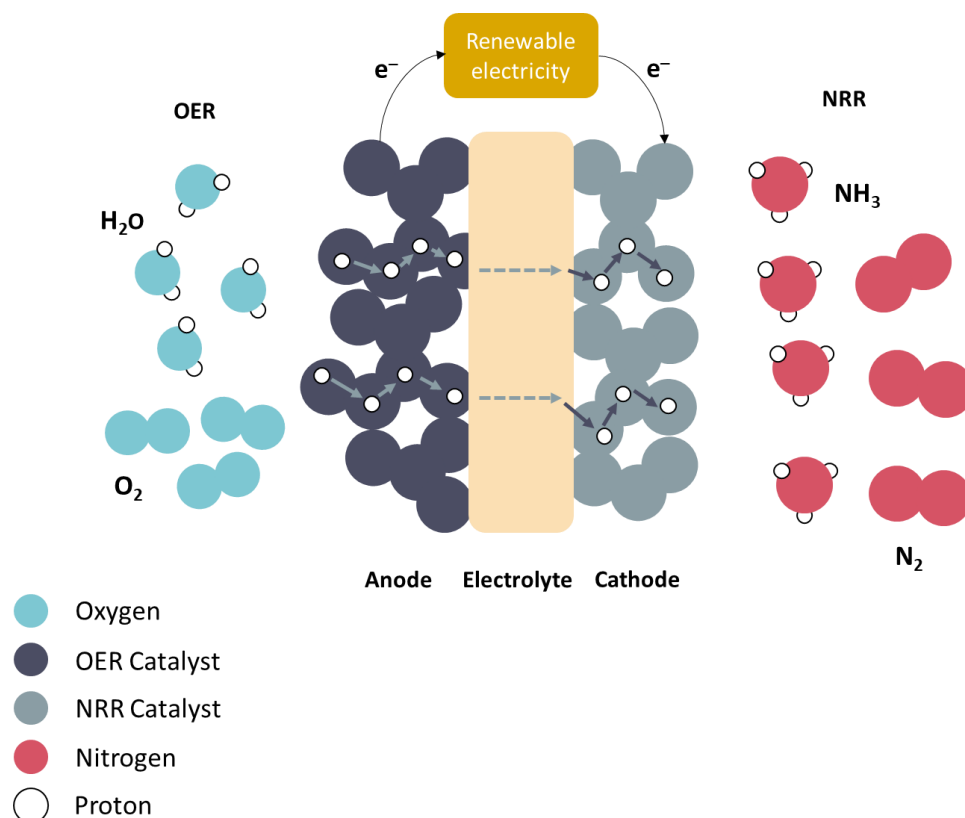


Figure 1. Schematic of the PCEC setup designed for NH_3 synthesis, wherein H_2O and N_2 are transformed into NH_3 .

The three essential components of a PCEC are an electrolyte, an anode, and a cathode (Figure 1). The electrolyte serves as an ion conductor that separates the electrodes and facilitates ion transport. The electrochemical reactions within the PCEC are non-spontaneous, implying that they do not occur naturally; an external influence, typically electricity, is necessary to drive the reactions [17].

Anode reaction

- At the anode, an electric current passes through water, thereby splitting water molecules into hydrogen (protons) and oxygen ions.
- Reaction: $2\text{H}_2\text{O} \rightarrow \text{O}_2 + 4\text{H}^+ + 4\text{e}^-$

Electron and proton transport:

- Electrons generated at the anode during water splitting are transported through an external electric circuit.
- Protons generated at the anode during water splitting are transported through the electrolyte [18].

Cathode reaction

- At the cathode, protons (H^+) from the anode and nitrogen atoms react to produce NH_3
- Reaction: $\text{N}_2 + 3\text{H}^+ + 3\text{e}^- \rightarrow \text{NH}_3$

Based on their supporting materials, high-temperature fuel cells can be categorized into three types: (i) cathode-, (ii) electrolyte-, and (iii) anode-supported. They are named based on the component that is fabricated first, which is generally the thickest component [19]. In this review, we focus only on electrolyte-supported cells. Despite the lower ohmic losses and power densities, anode-supported cells are difficult to fabricate on a large scale owing to the highly porous support and high manufacturing costs [20–23].

A seminal review by Giddey et al. provided a comprehensive overview of material construction, major technical challenges, and the technological landscape in the field [12]. However, the reaction conditions were not broadly defined. Garagounis et al. extensively reviewed solid-state NH_3 synthesis, particularly in PCECs [13]. Another review by Medvedev et al. in 2019 focused on NH_3^- and H_2^- producing PCECs, emphasizing design parameters such as thickness, partial pressure of H_2O , and other operational conditions such as polarization loss, ohmic loss, thermoneutral voltage, and open-circuit voltage [16].

We observed a gap in research involving N_2 at the cathode and only H_2O at the anode, except for the study by Yun et al. [24], which will be discussed subsequently. In another study, although $26.8 \text{ nmol NH}_3 \text{ s}^{-1} \text{ cm}^{-2}$ was achieved using N_2 at the cathode and H_2O at the anode, expensive plasma-assisted technology was employed [25]. Most studies focused on mixtures of H_2O and H_2 . Among them, the highest NH_3 production rate of $14 \text{ mol}^{-9} \text{ cm}^{-2} \text{ s}^{-1}$ was reported by Chien et al. [26]. Figure 2 depicts the questions that we aim to answer through this review.

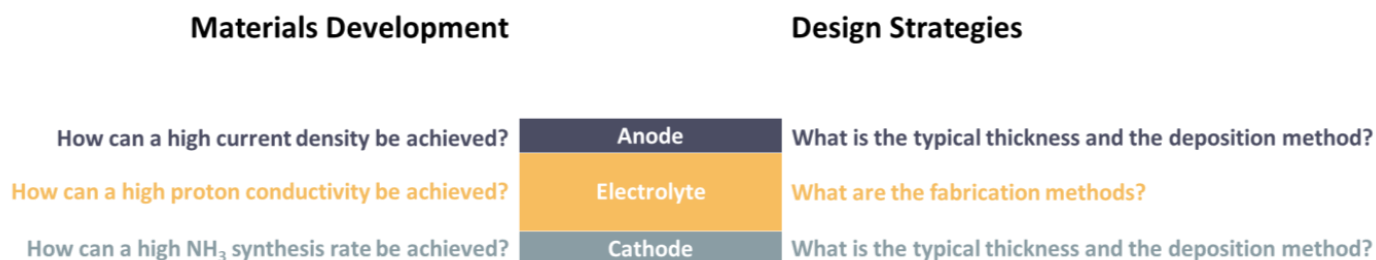


Figure 2. Questions to be answered through this review.

In this review, we summarize the existing design strategies in terms of electrolyte fabrication and properties, in addition to the electrocatalytic performance based on the NH_3 synthesis rate, Faradaic efficiency, and current density. Furthermore, the NRR and

OER mechanisms are discussed to address prevalent challenges. Finally, we highlight the challenges encountered in the development of PCEC devices and provide directions for further advancements in this technology.

2. Reaction Mechanism

For further advancements in the OER and NRR, the underlying mechanisms must be elucidated. Figure 3 provides a visual representation of the four primary pathways involved in N_2 reduction and NH_3 production in the PCECs.

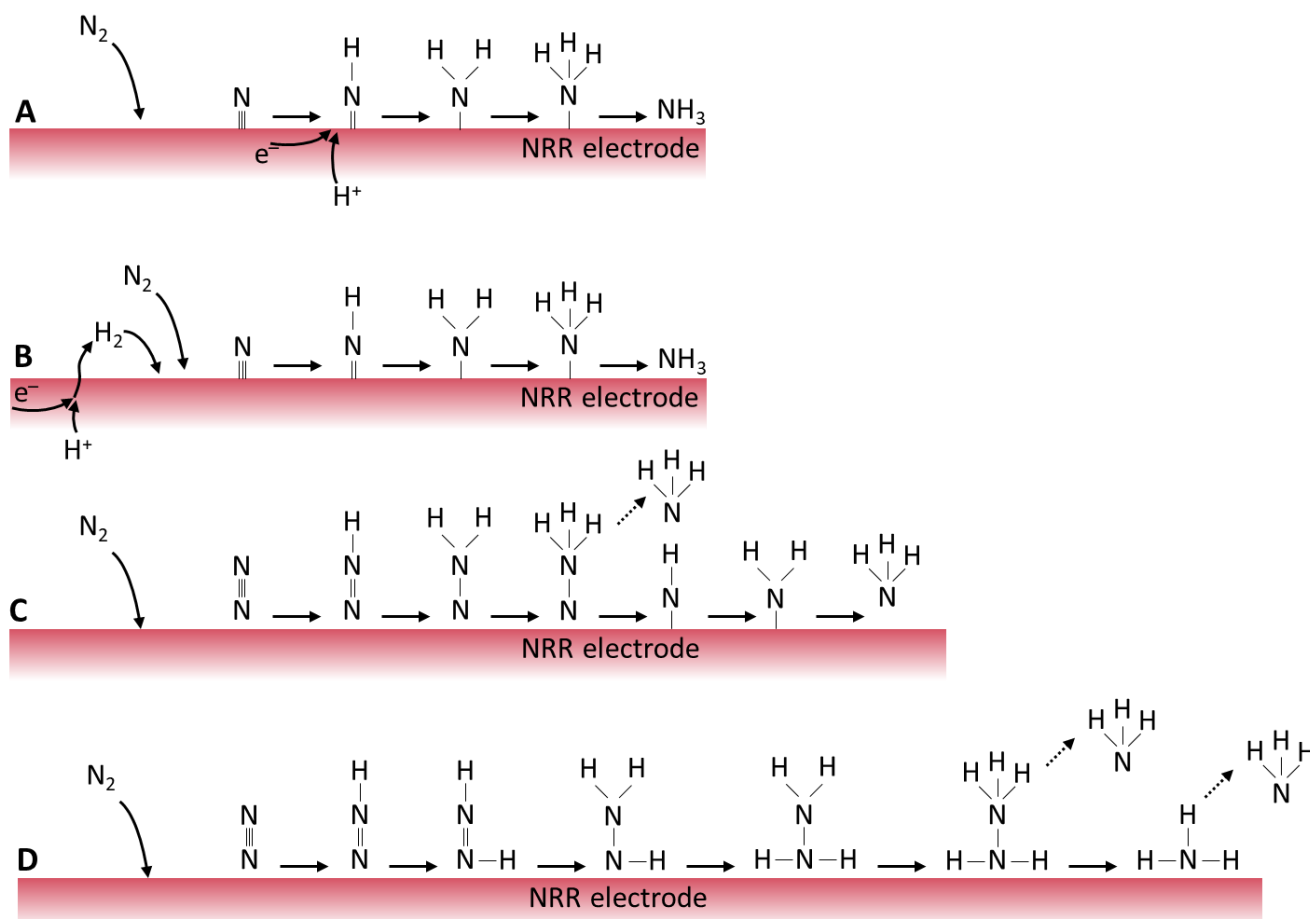


Figure 3. Potential NRR pathways in PCECs. Adapted from Duan et al. [11]. The solid one is for adsorbed atom while the dotted line is for desorbed atom.

Pathway A illustrates the electrochemical NH_3 synthesis through a dissociative mechanism, wherein protons directly combine with electrons to reduce the adsorbed N_2 on the catalyst, thereby producing NH_3 . In contrast to conventional methods, this direct electrochemical NH_3 synthesis method does not require a stoichiometric amount of gaseous H_2 , resulting in a considerably higher Faradaic selectivity. To enhance Pathway A, the NRR electrode should inhibit the hydrogen evolution reaction (HER) while maintaining sufficient electrocatalytic activity for N_2 reduction.

In contrast, Pathway B represents the conventional Haber–Bosch (HB) reaction, wherein N_2 is reduced by gaseous H_2 produced through the HER. Here, thermochemical catalytic NH_3 synthesis primarily governs NH_3 production. Therefore, the H_2/N_2 ratio is instrumental in determining the NH_3 production rate because it follows the thermodynamics of thermochemical NH_3 synthesis. Increasing the NH_3 yield requires the PCECs to operate at a high current density to ensure that the H_2/N_2 ratio is approximately 3/1. However, under such conditions, the NH_3 Faradaic selectivity is low because a substantial amount of H_2 remains unused.

In the N_2 adsorption depicted by Pathway C, the $N\equiv N$ bond remains intact after N_2 adsorption until a specific step in the hydrogenation process [27]. In contrast, in Pathway D, hydrogenation occurs alternately on two nitrogen atoms, and the $N\equiv N$ bond breaks only in the final step, thus forming the first NH_3 molecule; another NH_3 molecule remains bonded to the surface of the catalyst. These pathways help to clarify the complex mechanisms governing NH_3 production in PCECs [28–33].

The OER mechanism must be investigated in addition to the NRR mechanism. Liu et al. conducted a comprehensive study based on density functional theory calculations to elucidate the OER on $La_{0.6}Sr_{0.4}Ce_{0.2}Fe_{0.8}O_{3-\delta}$ catalysts, which are prominent catalysts wherein cobalt is doped in high-entropy perovskites. Figure 4 illustrates the potential OER pathway in PCECs. Their study revealed the following steps in the OER mechanism [34]:

- (i) The reaction is initiated when a water molecule is adsorbed on the catalyst surface.
- (ii) Consequently, surface-bound hydroxyl species (HO^*) are formed.
- (iii) The generated HO^* decomposes into hydrogen (H^*) and oxygen (O^*) species.
- (iv) Protons (H^+) are transferred to the cathode through the electrolyte.
- (v) Finally, gaseous oxygen materializes through desorption [35].

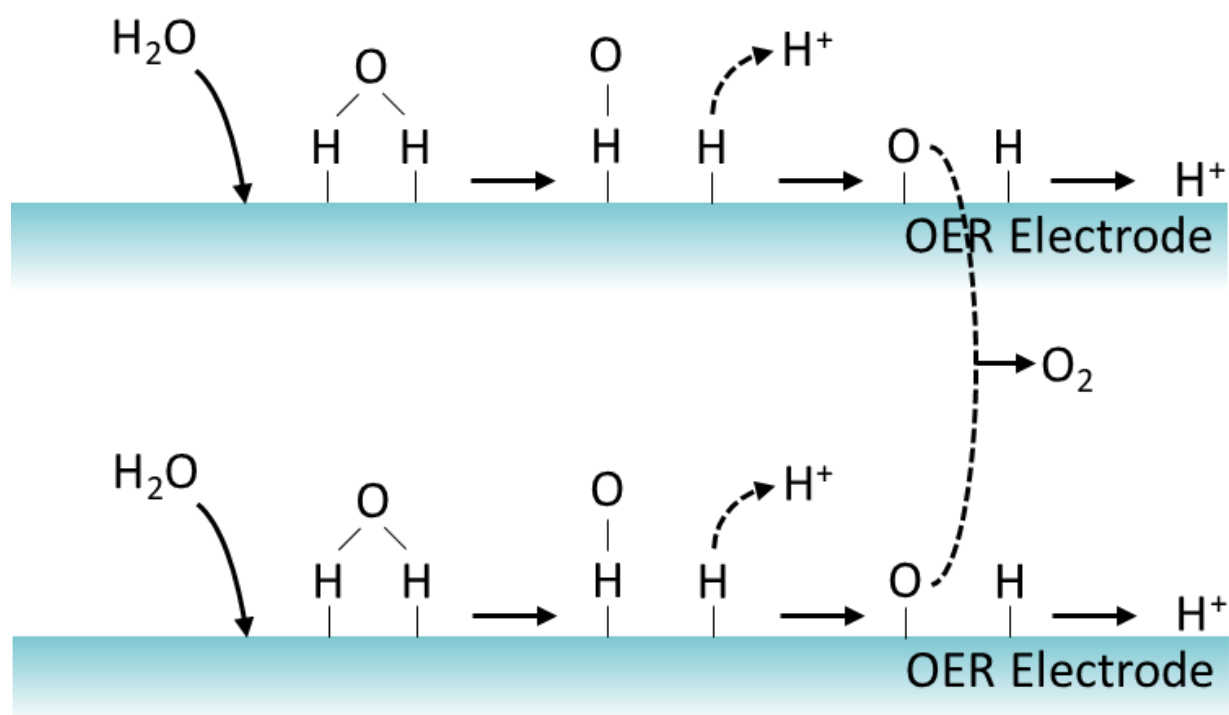


Figure 4. Potential OER pathway in PCECs. The solid one is for adsorbed atom while the dotted line is for desorbed atom.

The analysis of the OER catalytic mechanism elucidates the intricate processes that govern efficient OERs. By investigating the intricate interplay between surface sites, reaction intermediates, and electron transfer pathways, we can acquire a deeper understanding of the underlying principles driving the catalytic activity. This can facilitate the optimal design of catalysts and contribute to the broader field of sustainable energy conversion.

Continued research can potentially reveal more nuances in the OER mechanism. Our models and predictions can be refined by integrating advanced experimental techniques and computational approaches, ultimately promoting the development of catalysts with enhanced performance and durability. Addressing the challenges associated with the OER mechanism will enable renewable energy technologies to be utilized more efficiently.

3. PCEC Design Strategies

High-temperature cells such as solid oxide fuel cells (SOFCs) have been extensively designed [14]. However, selecting an appropriate design for each application is important because the cell performance strongly depends on the cathode, anode, and electrolyte materials. Medvedev discussed the influence of the design strategies on the performance of H₂-producing PCECs [16]. However, PCEC design strategies for NH₃ synthesis are limited. This section describes the fabrication and design strategies for the electrolyte and electrodes.

3.1. Electrolyte Design Strategies

The electrolyte is considered the most important component of a PCEC, particularly in electrolyte-supported systems because it occupies the largest volume. BaCeO₃ and BaZrO₃-based materials have been reported to be good protonic conductors [20]. Although BaCeO₃ exhibits high conductivity, BaZrO₃ provides better stability. Furthermore, Ce and Zr have been mixed with other dopants, such as Y and Yb, resulting in the well-known BaZr_{0.4}Ce_{0.4}Y_{0.1}Yb_{0.1}O_{3-δ} (BZCYYB 4411) and BaZr_{0.1}Ce_{0.7}Y_{0.1}Yb_{0.1}O_{3-δ} (BZCYYb 1711) electrolytes [21,22]. In general, a higher Ce content increases the proton conductivity, whereas a higher Zr content increases the stability [23,36]. In a PCEC, the applied electrical current serves two potential pathways: proton and electron transfers. The primary objective of a PCEC is to facilitate the movement of protons (H⁺) from the OER to the NRR sides, where they participate in hydrogen production. However, electron transfer, in which electrons move instead of protons, can be detrimental to the cell performance. This is because electron transfer reduces the Faradaic efficiency of the cell; particularly, a portion of the electrical energy is redirected to unintended reactions, leading to energy losses and potentially reducing the overall hydrogen production efficiency. Increasing the Ce content increases the protonic transference number and decreases the electron transference number. Therefore, BZCYYb 1711 is more suitable for PCECs than BZCYYb 4411 [37].

This discussion pertains to three distinct electrolyte forms: pellets, thin films, and columnar structures. Pellet-type electrolytes have been extensively used in fuel cells and batteries [38,39]. They are relatively easy to manufacture and integrate into PCEC stacks [40]. This method involves placing a few grams of electrolyte powder into a mold, which is typically cylindrical, and ultimately shaping it into a coin-like pellet. This conventional approach has resulted in considerable advancements in terms of electrolyte composition. The details of various pellet electrolytes developed thus far are listed in Table 1.

Table 1. Conductivities of proton-conducting electrolytes and their synthesis methods.

Electrolyte	Method	Conductivity (S cm ⁻¹)	Thickness (mm)	Reference
SrCe _{0.95} Yb _{0.05} O _{3-δ}	sol-gel	Unknown	1.5	[41]
BaZr _{0.8-x-y} Ce _x Nd _y Y _{0.1} Yb _{0.1} O _{3-δ}	Pechini method	500 °C: 3.77 × 10 ⁻⁴	0.8–1.5	[42]
BaZr _{0.85} Y _{0.15} O _{3-δ}	hydrothermal process	600 °C: 2.5 × 10 ⁻³	1.6	[43]

While the solid-state reaction is common for powder preparation, sol-gel or glycine nitrate processes are commonly employed to obtain finer particles and higher peak power densities [42]. The pellet electrolyte thickness is in the range of 0.8–1.6 mm (Table 1). Medvedev suggested that thin-film technology must be developed for the electrochemical synthesis of NH₃ [16]. With reference to the electrolyte properties, the thickness plays a crucial role in determining both the ohmic resistance and electron transport characteristics. Thicker electrolytes increase the ohmic resistance, whereas thinner electrolytes increase contact resistance at the electrolyte/electrode interface. In conventional electrolytes, the ohmic resistance tends to increase. This limitation can be effectively addressed using thin-film electrolytes [44]. Recent advancements in thin-film electrolytes for PCECs have been comprehensively presented in Table 2.

Table 2. Conductivities of thin-film electrolytes and their deposition/synthesis methods.

Electrolyte	Method	Conductivity (S cm ⁻¹)	Thickness (μm)	Reference
BaCe _{0.7} Zr _{0.1} Y _{0.2}	co-precipitation	650 °C: 2.8 × 10 ⁻²	~20	[45]
	solid-state reaction			
	dip-coating			
BaCe _{0.8} Y _{0.2-x} Nd _x O _{3-δ}	citrate–nitrate combustion	350 °C: 8.5 × 10 ⁻³	~20	[46]
BaCe _{1-x} In _x O _{3-δ}	auto-combustion reaction	700 °C: 5 × 10 ⁻³	20–25	[47]
BaZr _{0.1} Ce _{0.7} Y _{0.1} Yb _{0.1}	solid-state reaction	500 °C: 1.2 × 10 ⁻²	10	[48]
BaHf _{0.8} Yb _{0.2} O _{3-δ}	pulsed laser deposition (PLD)	500 °C: 2.5 × 10 ⁻³	110	[48]
BaZr _{0.1} Ce _{0.7} Y _{0.1} Yb _{0.1}	solid-state reaction	500 °C: 1.3 × 10 ⁻²	~10	[22]
BaZr _{0.4} Ce _{0.4} Y _{0.1} Yb _{0.1}	solid-state reaction	500 °C: 5.6 × 10 ⁻³	~15	[21]
BaZr _{0.2} Ce _{0.6} Y _{0.1} Yb _{0.1} O _{3-δ}	Pechini method	600 °C: 24.39	1	[49]
	inkjet printing			
BaCe _{0.5} Zr _{0.35} Y _{0.15} O _{3-δ}	citric nitrate method	Unknown	2–4	[50]
	PLD			
BaZr _{1-x-y} Ce _x Y _y O ₃	ultrafast microwave-assisted	Unknown	~12	[51]
	sintering			
BaZr _{0.2} Ce _{0.6} Y _{0.2} O ₃	tape casting	800 °C: 1 × 10 ⁻²	~7	[52]
	solid-state reaction			
BaCe _{0.55} Zr _{0.3} Y _{0.15} O _{3-δ}	spin coating	Unknown	~2.5	[53]
	screen printing			

The technological advancements in thin-film electrolytes are attributed to their reduced dimensions. Various deposition techniques, such as inkjet printing, pulsed layer deposition (PLD), tape casting, spin coating, and screen printing, are involved [49–53]. Screen printing and spin coating are known to be simple. However, considerable material wastage occurs, with a minimum thickness of approximately 10 μm. Furthermore, PLD, which is recognized for its effectiveness, requires complex operation and energy-intensive vacuum conditions. Inkjet printing offers the advantage of producing highly uniform surfaces with a minimum thickness of just 0.83 μm [49].

BaZr_{0.1}Ce_{0.7}Y_{0.1}Yb_{0.1} is an extensively investigated proton-conducting electrolyte, although some researchers have diverged, advocating other compositions as the most studied [22,45,47]. Some researchers have explored doping with elements such as Nd, Sc, In, and Hf, in addition to Y and Yb, to enhance the stability and sinterability of the electrolyte [22,43,44,46,48,54]. Ding et al. introduced a novel approach by ball milling, pelletizing, calcining, and crushing the pellets to produce a pure-phase powder on a relatively large scale (up to 4 kg per batch) [55]. Another approach involves combining all BZCYb1711 nitrate precursors in deionized water, followed by the addition of a specific quantity of NaOH. NaOH reacts with nitrates and forms mixed metal hydroxides before calcination, which produce mixed metal oxides (perovskite). This mixture is washed and then subjected to a high-temperature solid-state reaction [54]. The conventional box furnace method at 1000–1500 °C with a ramp of 1–5 °C min⁻¹ is typically used for sintering. Spark plasma and microwave sintering have been examined for rapid high-temperature results, with the aim of matching or surpassing the performance of conventional sintering [47,56].

The previous discussion encompassed two distinct electrolyte types (Figure 5), namely, the planar type (pellet and thin film), which necessitates sealing agents for the reactor connection, and the tubular configuration, which operates seamlessly without requiring sealing. Columnar electrolytes can be fabricated by templating using plaster molds or by rolling a thin-film electrolyte. Notably, columnar electrolytes have been employed in SOFCs [57–59]. Table 3 lists examples of columnar electrolyte utilization.

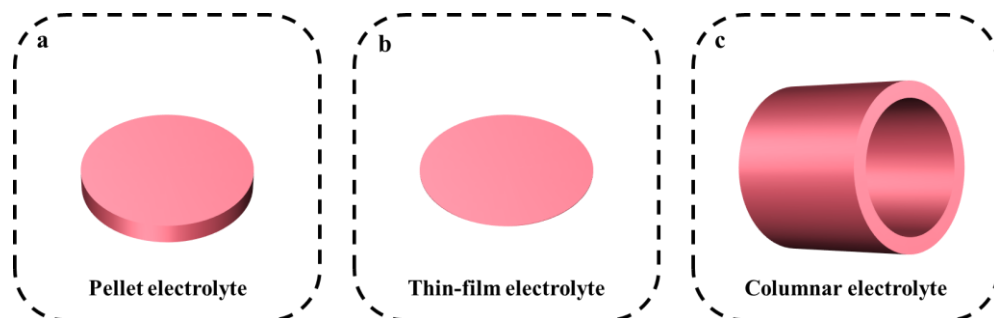


Figure 5. Illustration of (a) pellet, (b) thin-film, and (c) columnar electrolytes.

Table 3. Conductivities of columnar electrolytes and their deposition/synthesis method.

Electrolyte	Method	Conductivity	Reference
$\text{BaZr}_{0.4}\text{Ce}_{0.4}\text{Y}_{0.15}\text{Zn}_{0.05}\text{O}_3$	solid-state reaction	Unknown	[60]
$\text{BaZr}_{0.1}\text{Ce}_{0.7}\text{Y}_{0.1}\text{Yb}_{0.1}$	solid-state reaction	Unknown	[61]

3.2. Electrode Design Strategies

In contrast to thermochemical catalysts, electrocatalysts must be pretreated to ensure that they can mechanically bond to the electrolyte while remaining catalytically active. In electrolyte-supported cells, the cathode and anode are deposited on opposite sides of the cell. The difference between the anode and cathode materials makes it necessary to specify the method that should be used to deposit them onto the electrolyte.

Recently, various conventional and ambient-condition deposition methods, such as the doctor blade method, drop coating, screen printing, tape casting, and spray coating, have been used to develop electrode materials for PCECs (Table 4). Although these methods are simple, the electrode thickness is controlled only through a randomized parameter, such as printing passes or number of drops. Therefore, many researchers have recently employed PLD to produce a smooth electrode surface and ensure good interfacial contact between the electrolyte and electrode [62].

Table 4. Deposition methods and electrode thickness in key research on OER and NRR catalysts.

Cathode	Deposition Method	Thickness (μm)	Reference
$\text{La}_{0.6}\text{Sr}_{0.4}\text{Co}_{0.2}\text{Fe}_{0.8}\text{O}_{3-\delta}$	Unknown	44	[24]
Ag	-	4	
Pt	-	8	
Fe	doctor blade	15–25	[26]
10-Fe-BCY	doctor blade	15–25	
0.5W-10Fe-BCY	doctor blade	15–25	
$\text{PrBa}_{0.5}\text{Sr}_{0.5}\text{Co}_{1.5}\text{Fe}_{0.5}\text{O}_{5+\delta}$	-	10–20	[36]
Ru–Ag/MgO	Unknown	-	[41]
Ni-BCYR	-	-	[63]
$\text{NdBa}_{0.5}\text{Sr}_{0.5}\text{Co}_{1.5}\text{Fe}_{0.5}\text{O}_{5+\delta}$ (NBSCF)-BZCYYb	drop coating	15	[64]
Pr_2NiO_4 -BZCY	screen printing	13	[65]
$\text{PrCo}_{0.05}\text{Ni}_{0.5}\text{O}_{3-\delta}$	tape casting	29	[66]
$\text{Ba}_{0.9}\text{Co}_{0.7}\text{Fe}_{0.2}\text{Nb}_{0.1}\text{O}_{3-\delta}$	screen printing	15	[67]
$\text{Pr}_{0.2}\text{Ba}_{0.2}\text{Sr}_{0.2}\text{La}_{0.2}\text{Ca}_{0.2}\text{CoO}_{3-\delta}$	spray coating	20	[68]
$\text{PrBa}_{0.5}\text{Sr}_{0.5}\text{Co}_{1.5}\text{Fe}_{0.5}\text{O}_{5+\delta}$	PLD	20	[69]
$\text{Gd}_{0.3}\text{Ca}_{2.7}\text{Co}_{3.82}\text{Cu}_{0.18}\text{O}_{9-\delta}$	screen printing	30	[70]

4. Current Progress

The NRR and OER have been studied extensively; the catalysts used for these reactions are summarized in Tables 5 and 6, respectively.

Table 5. Notable NRR catalysts in PCECs for NH₃ synthesis.

Cathode *	Electrolyte	NH ₃ Production Rate [mol cm ⁻² s ⁻¹] × 10 ⁻⁹	Thickness (μm)	Reference
La _{0.6} Sr _{0.4} Co _{0.2} Fe _{0.8} O _{3-δ}	BaZr _{0.8} Y _{0.2} O _{3-δ}	0.0850	44	[24]
Ag	BaZr _{0.8} Y _{0.2} O _{3-δ}	0.0490	4	
Pt	BaZr _{0.8} Y _{0.2} O _{3-δ}	<0.0010	8	
Fe	BaCe _{0.9} Y _{0.1} O _{3-δ}	14.000	15–25	[26]
10-Fe-BCY	BaCe _{0.9} Y _{0.1} O _{3-δ}	0.4200	15–25	
0.5W-10Fe-BCY	BaCe _{0.9} Y _{0.1} O _{3-δ}	0.5700	15–25	
Ru–Ag/MgO	SrCe _{0.95} Yb _{0.05} O _{3-δ}	0.0003	-	[41]
Ni-BCYR	BaCe _{0.9} Y _{0.1} O _{3-δ}	0.0110	-	[63]

* only for OER coupled with NRR configuration.

Table 6. Notable OER catalysts in PCECs for NH₃ synthesis.

Anode	Electrolyte	Current Density @1.3 V and 550 °C [A cm ⁻²]	Thickness (μm)	Reference
Pr _{0.2} Ba _{0.2} Sr _{0.2} La _{0.2} Ca _{0.2} CoO _{3-δ}	BaZr _{0.1} Ce _{0.7} Y _{0.1} Yb _{0.1} O _{3-δ}	−0.800	20	[68]
PrBa _{0.5} Sr _{0.5} Co _{1.5} Fe _{0.5} O _{5+δ}	BaZr _{0.4} Ce _{0.4} Y _{0.1} Yb _{0.1} O _{3-δ}	−1.059	20	[69]
Gd _{0.3} Ca _{2.7} Co _{3.82} Cu _{0.18} O _{9-δ}	BaZr _{0.1} Ce _{0.7} Y _{0.1} Yb _{0.1} O _{3-δ}	−1.241	30	[70]

Based on Table 5, metallic catalysts evidently yield higher reaction rates. This could be attributed to two main factors. First, perovskite-based electrocatalysts may possibly be affected by degradation at the interface and thermal mismatch with the electrolyte, thus decreasing the performance [24]. Second, the electrochemical promotion of catalysis is more pronounced in pure metal catalysts with a higher effective double layer (*S**_{eff}) on their surfaces than in supported electrocatalysts [26]. However, pure metallic catalysts are typically expensive.

Ru is regarded as a suitable catalyst for thermochemical NH₃ synthesis because of its peak position on Skulason's volcano diagram, which shows that it requires a minimum potential for electrochemical NH₃ synthesis. It has also been reported to be an ultra-efficient electrocatalyst for the NRR, with a lower reduction potential than that of Fe [71–75]. However, Ag is a more cost-effective option because of its natural abundance. Although noble-metal-based electrocatalysts exhibit favorable activity, efficiency, and selectivity, their practical application is inhibited by their high cost and scarcity [27]. Consequently, extensive research has been conducted on transition-metal-based electrocatalysts for the NRR. The NH₃ synthesis rate of Pt catalysts can be primarily attributed to their strong HER activity [76,77]. At negative potentials, the surface of Pt nanoparticles tends to adsorb hydrogen atoms rather than nitrogen atoms, thus affecting the overall performance [78].

Considering NH₃-producing PCECs, most studies have only focused on the NRR, whereas the OER has been overlooked. The NH₃ synthesis reaction is typically performed at 475–600 °C [24]. Pei et al. briefly summarized the OER performance at a cell voltage of 1.3 V and operating temperature of 550 °C [67].

Currently, transition metals, particularly compounds based on Fe, Co, and Ni, have demonstrated remarkable catalytic activity for the OER [79]. A successful method to enhance the OER activity involves altering the surface electronic structure through the addition of supporting materials to the active metal (Fe, Co, or Ni). This strategy has attracted attention, particularly with reference to multi-metal materials such as high-entropy perovskites, because they provide numerous possibilities for modifying the characteristics and improving the catalytic performance [80].

Among multi-metal materials, Co-based double perovskite oxides are notable for their rapid ion diffusion and enhanced surface catalysis, resulting in high electrochemical performance in single cells [35,69,81]. Various studies have explored the application of OER catalysts in PCECs (Table 6). For example, $\text{Gd}_{0.3}\text{Ca}_{2.7}\text{Co}_{3.82}\text{Cu}_{0.18}\text{O}_{9-\delta}$ exhibits the highest current density owing to various factors, including abundant oxygen vacancies in the central Co–O layer of the $\text{Ca}_3\text{Co}_2\text{O}_3$ rock–salt subsystem, which alters the electronic charge carrier concentration. The needlelike grain morphology aids in the complex flow of the reaction components via triple conduction and open diffusion paths [70].

Despite the promising characteristics of Co-based double perovskite oxides, these high-entropy perovskite oxides have disadvantages such as instability, thermal mismatch, and high cost, which limit their widespread implementation [35,69,81,82]. Thermal mismatch occurs when the OER catalyst and electrolyte materials have different coefficients of thermal expansion (CTE). The CTE indicates the extent to which a material expands when exposed to changes in temperature. If the OER catalyst and electrolyte have significantly different CTE, they may expand at different rates as the temperature changes [83]. Therefore, catalysts with compatible mechanical properties need to be used.

5. Conclusions

This review presented a comprehensive outline of the design strategies for PCECs aimed at enhancing electrochemical NH_3 synthesis. The mechanisms of the reactions involved were delineated, and design strategies for PCECs were investigated. This review provides novel insights into catalyst development for the NRR and OER. The following points summarize our findings and recommendations to further develop this technology.

Electrolytes must be further developed in terms of their architecture and thickness. For electrodes, understanding the underlying reaction mechanisms is essential. Co-based double perovskite oxides display rapid ion diffusion and improved surface catalysis, resulting in excellent electrochemical performance in individual cells. However, their application is challenging owing to high-entropy perovskite instability, thermal mismatch, and high cost. Computational analysis is indispensable when investigating the reaction mechanisms, particularly in the context of employing high-entropy perovskites as OER catalysts. Based on this review, we recommend the following research directions:

1. A more scalable approach must be investigated to deposit Fe- and Co-based perovskite electrodes to reduce catalyst wastage.
2. A more complex catalyst must be developed for the NRR because existing materials are not as advanced as OER catalysts.
3. Stability and thermal mismatch issues for the OER must be addressed to decrease wastage and increase cell stability.

We believe that investigating more scalable methods, such as atomic layer deposition, will enhance the positive environmental impact of electrochemical catalysts used for NH_2 synthesis. Similar to thermochemical NH_3 synthesis catalysts, investigating various support materials for Fe- or Ru-based catalysts can be beneficial for the NRR. For further advancements in OER catalysts, the stability of the catalyst must be improved, and the thermal mismatch must be eliminated to enhance the overall efficiency of the PCEC.

Author Contributions: Conceptualization, H.M.V.; investigation, M.-C.K.; writing—original draft preparation, H.M.V.; writing—review and editing, A.B.; visualization, H.M.V.; supervision, S.H.C.; funding acquisition, S.H.C. All authors have read and agreed to the published version of the manuscript.

Funding: This work was supported by the National Research Foundation of Korea (NRF), funded by the Korean Government (Ministry of ICT) [Grant No. 2021R1A2C2008662].

Data Availability Statement: Data are contained within the article.

Acknowledgments: We would like to thank the Korea Institute of Science and Technology for facilitating this work.

Conflicts of Interest: The authors declare no conflicts of interest.

References

1. Teichmann, D.; Stark, K.; Müller, K.; Zöttl, G.; Wasserscheid, P.; Arlt, W. Energy Storage in Residential and Commercial Buildings via Liquid Organic Hydrogen Carriers (LOHC). *Energy Environ. Sci.* **2012**, *5*, 9044–9054. [CrossRef]
2. Kandemir, T.; Schuster, M.E.; Senyshyn, A.; Behrens, M.; Schlögl, R. The Haber–Bosch Process Revisited: On the Real Structure and Stability of “Ammonia Iron” under Working Conditions. *Angew. Chem. Int. Ed.* **2013**, *52*, 12723–12726. [CrossRef] [PubMed]
3. Haber, F.; Rossignol, R. Le Über Die Technische Darstellung von Ammoniak Aus Den Elementen. *Zeitschrift für Elektrochemie und Angew. Phys. Chemie* **1913**, *19*, 53–72. [CrossRef]
4. Aika, K.i.; Hori, H.; Ozaki, A. Activation of Nitrogen by Alkali Metal Promoted Transition Metal I. Ammonia Synthesis over Ruthenium Promoted by Alkali Metal. *J. Catal.* **1972**, *27*, 424–431. [CrossRef]
5. IEA Ammonia Technology Roadmap. Available online: <https://www.iea.org/reports/ammonia-technology-roadmap> (accessed on 4 October 2023).
6. Brown, T. Feeding Life 2030: The Vision of Fertilizers Europe. Available online: <https://www.ammoniaenergy.org/articles/feeding-life-2030-the-vision-of-fertilizers-europe/> (accessed on 4 October 2023).
7. Shipman, M.A.; Symes, M.D. Recent Progress towards the Electrosynthesis of Ammonia from Sustainable Resources. *Catal. Today* **2017**, *286*, 57–68. [CrossRef]
8. Foster, S.L.; Bakovic, S.I.P.; Duda, R.D.; Maheshwari, S.; Milton, R.D.; Minter, S.D.; Janik, M.J.; Renner, J.N.; Greenlee, L.F. Catalysts for Nitrogen Reduction to Ammonia. *Nat. Catal.* **2018**, *1*, 490–500. [CrossRef]
9. Jeerh, G.; Zhang, M.; Tao, S. Recent Progress in Ammonia Fuel Cells and Their Potential Applications. *J. Mater. Chem. A* **2021**, *9*, 727–752. [CrossRef]
10. Gunduz, S.; Deka, D.J.; Ozkan, U.S. A Review of the Current Trends in High-Temperature Electrocatalytic Ammonia Production Using Solid Electrolytes. *J. Catal.* **2020**, *387*, 207–216. [CrossRef]
11. Liu, F.; Ding, D.; Duan, C. Protonic Ceramic Electrochemical Cells for Synthesizing Sustainable Chemicals and Fuels. *Adv. Sci.* **2023**, *10*, e2206478. [CrossRef]
12. Giddey, S.; Badwal, S.P.S.; Kulkarni, A. Review of Electrochemical Ammonia Production Technologies and Materials. *Int. J. Hydrogen Energy* **2013**, *38*, 14576–14594. [CrossRef]
13. Garagounis, I.; Kyriakou, V.; Skodra, A.; Vasileiou, E.; Stoukides, M. Electrochemical Synthesis of Ammonia in Solid Electrolyte Cells. *Front. Energy Res.* **2014**, *2*, 1. [CrossRef]
14. Wang, B.; Li, T.; Gong, F.; Othman, M.H.D.; Xiao, R. Ammonia as a Green Energy Carrier: Electrochemical Synthesis and Direct Ammonia Fuel Cell—A Comprehensive Review. *Fuel Process. Technol.* **2022**, *235*, 107380. [CrossRef]
15. Juangsa, F.B.; Irhamna, A.R.; Aziz, M. Production of Ammonia as Potential Hydrogen Carrier: Review on Thermochemical and Electrochemical Processes. *Int. J. Hydrogen Energy* **2021**, *46*, 14455–14477. [CrossRef]
16. Medvedev, D. Trends in Research and Development of Protonic Ceramic Electrolysis Cells. *Int. J. Hydrogen Energy* **2019**, *44*, 26711–26740. [CrossRef]
17. Shen, H.; Choi, C.; Masa, J.; Li, X.; Qiu, J.; Jung, Y.; Sun, Z. Electrochemical Ammonia Synthesis: Mechanistic Understanding and Catalyst Design. *Chem* **2021**, *7*, 1708–1754. [CrossRef]
18. Trivinho-Strixino, F.; Santos, J.S.; Souza Sikora, M. 3—Electrochemical Synthesis of Nanostructured Materials. In *Nanostructures*; Da Róz, A.L., Ferreira, M., de Lima Leite, F., Oliveira, O.N.B.T.-N., Eds.; William Andrew Publishing: Norwich, NY, USA, 2017; pp. 53–103, ISBN 978-0-323-49782-4.
19. Droushiotis, N.; Grande, F.D.; Dzarfan Othman, M.H.; Kanawka, K.; Doraswami, U.; Metcalfe, I.S.; Li, K.; Kelsall, G. Comparison between Anode-supported and Electrolyte-supported Ni-CGO-LSCF Micro-tubular Solid Oxide Fuel Cells. *Fuel Cells* **2014**, *14*, 200–211. [CrossRef]
20. Iwahara, H. Oxide-Ionic and Protonic Conductors Based on Perovskite-Type Oxides and Their Possible Applications. *Solid State Ionics* **1992**, *52*, 99–104. [CrossRef]
21. Choi, S.; Kucharczyk, C.J.; Liang, Y.; Zhang, X.; Takeuchi, I.; Ji, H.I.; Haile, S.M. Exceptional Power Density and Stability at Intermediate Temperatures in Protonic Ceramic Fuel Cells. *Nat. Energy* **2018**, *3*, 202–210. [CrossRef]
22. Liu, M.; Yang, L.; Wang, S.; Blinn, K.; Liu, M.; Liu, Z.; Cheng, Z. Enhanced Sulfur and Coking Tolerance of a Mixed Ion Conductor for SOFCs: BaZr_{0.1}Ce_{0.7}Y_{0.2}–xYb_xO_{3–δ}. *Science* **2009**, *326*, 126–129. [CrossRef]
23. Zhu, H.; Kee, R.J. Membrane Polarization in Mixed-Conducting Ceramic Fuel Cells and Electrolyzers. *Int. J. Hydrogen Energy* **2016**, *41*, 2931–2943. [CrossRef]
24. Yun, D.S.; Joo, J.H.; Yu, J.H.; Yoon, H.C.; Kim, J.N.; Yoo, C.Y. Electrochemical Ammonia Synthesis from Steam and Nitrogen Using Proton Conducting Yttrium Doped Barium Zirconate Electrolyte with Silver, Platinum, and Lanthanum Strontium Cobalt Ferrite Electrocatalyst. *J. Power Sources* **2015**, *284*, 245–251. [CrossRef]

25. Sharma, R.K.; Patel, H.; Mushtaq, U.; Kyriakou, V.; Zafeiropoulos, G.; Peeters, F.; Welzel, S.; Van De Sanden, M.C.M.; Tsampas, M.N. Plasma Activated Electrochemical Ammonia Synthesis from Nitrogen and Water. *ACS Energy Lett.* **2021**, *6*, 313–319. [[CrossRef](#)]
26. Li, C.I.; Matsuo, H.; Otomo, J. Effective Electrode Design and the Reaction Mechanism for Electrochemical Promotion of Ammonia Synthesis Using Fe-Based Electrode Catalysts. *Sustain. Energy Fuels* **2021**, *5*, 188–198. [[CrossRef](#)]
27. Liu, D.; Chen, M.; Du, X.; Ai, H.; Lo, K.H.; Wang, S.; Chen, S.; Xing, G.; Wang, X.; Pan, H. Development of Electrocatalysts for Efficient Nitrogen Reduction Reaction under Ambient Condition. *Adv. Funct. Mater.* **2021**, *31*, 2008983. [[CrossRef](#)]
28. Huang, Y.; Babu, D.D.; Peng, Z.; Wang, Y. Atomic Modulation, Structural Design, and Systematic Optimization for Efficient Electrochemical Nitrogen Reduction. *Adv. Sci.* **2020**, *7*, 1902390. [[CrossRef](#)] [[PubMed](#)]
29. MacLeod, K.C.; Holland, P.L. Recent Developments in the Homogeneous Reduction of Dinitrogen by Molybdenum and Iron. *Nat. Chem.* **2013**, *5*, 559–565. [[CrossRef](#)]
30. Wang, Y.; Zhou, W.; Jia, R.; Yu, Y.; Zhang, B. Unveiling the Activity Origin of a Copper-Based Electrocatalyst for Selective Nitrate Reduction to Ammonia. *Angew. Chemie Int. Ed.* **2020**, *59*, 5350–5354. [[CrossRef](#)]
31. Han, J.; Liu, Z.; Ma, Y.; Cui, G.; Xie, F.; Wang, F.; Wu, Y.; Gao, S.; Xu, Y.; Sun, X. Ambient N₂ Fixation to NH₃ at Ambient Conditions: Using Nb₂O₅ Nanofiber as a High-Performance Electrocatalyst. *Nano Energy* **2018**, *52*, 264–270. [[CrossRef](#)]
32. Mars, P.; van Krevelen, D.W. Oxidations Carried out by Means of Vanadium Oxide Catalysts. *Chem. Eng. Sci.* **1954**, *3*, 41–59. [[CrossRef](#)]
33. Abghoui, Y.; Garden, A.L.; Howalt, J.G.; Vegge, T.; Skúlason, E. Electroreduction of N₂ to Ammonia at Ambient Conditions on Mononitrides of Zr, Nb, Cr, and V: A DFT Guide for Experiments. *ACS Catal.* **2016**, *6*, 635–646. [[CrossRef](#)]
34. Zhou, Y.; Zhang, W.; Kane, N.; Luo, Z.; Pei, K.; Sasaki, K.; Choi, Y.; Chen, Y.; Ding, D.; Liu, M. An Efficient Bifunctional Air Electrode for Reversible Protonic Ceramic Electrochemical Cells. *Adv. Funct. Mater.* **2021**, *31*, 2105386. [[CrossRef](#)]
35. Ding, D.; Zhang, Y.; Wu, W.; Chen, D.; Liu, M.; He, T. A Novel Low-Thermal-Budget Approach for the Co-Production of Ethylene and Hydrogen via the Electrochemical Non-Oxidative Deprotonation of Ethane. *Energy Environ. Sci.* **2018**, *11*, 1710–1716. [[CrossRef](#)]
36. Duan, C.; Kee, R.; Zhu, H.; Sullivan, N.; Zhu, L.; Bian, L.; Jennings, D.; O’Hayre, R. Highly Efficient Reversible Protonic Ceramic Electrochemical Cells for Power Generation and Fuel Production. *Nat. Energy* **2019**, *4*, 230–240. [[CrossRef](#)]
37. Han, D.; Liu, X.; Bjørheim, T.S.; Uda, T. Yttrium-Doped Barium Zirconate-Cerate Solid Solution as Proton Conducting Electrolyte: Why Higher Cerium Concentration Leads to Better Performance for Fuel Cells and Electrolysis Cells. *Adv. Energy Mater.* **2021**, *11*, 2003149. [[CrossRef](#)]
38. Zhu, J.; Li, X.L.; Wu, C.; Gao, J.; Xu, H.; Li, Y.; Guo, X.; Li, H.; Zhou, W. A Multilayer Ceramic Electrolyte for All-Solid-State Li Batteries. *Angew. Chemie Int. Ed.* **2021**, *60*, 3781–3790. [[CrossRef](#)] [[PubMed](#)]
39. Brett, D.J.L.; Aguiar, P.; Clague, R.; Marquis, A.J.; Schöttl, S.; Simpson, R.; Brandon, N.P. Application of Infrared Thermal Imaging to the Study of Pellet Solid Oxide Fuel Cells. *J. Power Sources* **2007**, *166*, 112–119. [[CrossRef](#)]
40. Feng, W.; Wu, W.; Jin, C.; Zhou, M.; Bian, W.; Tang, W.; Gomez, J.Y.; Boardman, R.; Ding, D. Exploring the Structural Uniformity and Integrity of Protonic Ceramic Thin Film Electrolyte Using Wet Powder Spraying. *J. Power Sources Adv.* **2021**, *11*, 100067. [[CrossRef](#)]
41. Skodra, A.; Stoukides, M. Electrocatalytic Synthesis of Ammonia from Steam and Nitrogen at Atmospheric Pressure. *Solid State Ionics* **2009**, *180*, 1332–1336. [[CrossRef](#)]
42. Yilmaz, S.; Kavici, B.; Ramakrishnan, P.; Celen, C.; Horri, B.A. Highly Conductive Cerium- and Neodymium-Doped Barium Zirconate Perovskites for Protonic Ceramic Fuel Cells. *Energies* **2023**, *16*, 4318. [[CrossRef](#)]
43. François, M.; Lescure, V.; Heintz, O.; Combemale, L.; Demoisson, F.; Caboche, G. Synthesis of Y-Doped BaZrO₃ Proton Conducting Electrolyte Material by a Continuous Hydrothermal Process in Supercritical Conditions: Investigation of the Formation Mechanism and Electrochemical Performance. *Ceram. Int.* **2023**, *49*, 25344–25352. [[CrossRef](#)]
44. Konwar, D.; Yoon, H.H. A Methane-Fueled SOFC Based on a Thin BaZr_{0.1}Ce_{0.7}Y_{0.1}Yb_{0.1}O_{3-δ} Electrolyte Film and a LaNi_{0.6}Co_{0.4}O₃ Anode Functional Layer. *J. Mater. Chem. A* **2016**, *4*, 5102–5106. [[CrossRef](#)]
45. Fan, Z.; Cao, D.; Zhou, M.; Zhu, Z.; Chen, M.; Liu, J. Barium Cerate-Zirconate Electrolyte Powder Prepared by Carbonate Coprecipitation for High Performance Protonic Ceramic Fuel Cells. *Ceram. Int.* **2023**, *49*, 8524–8532. [[CrossRef](#)]
46. Wang, S.; Shen, J.; Zhu, Z.; Wang, Z.; Cao, Y.; Guan, X.; Wang, Y.; Wei, Z.; Chen, M. Further Optimization of Barium Cerate Properties via Co-Doping Strategy for Potential Application as Proton-Conducting Solid Oxide Fuel Cell Electrolyte. *J. Power Sources* **2018**, *387*, 24–32. [[CrossRef](#)]
47. Malešević, A.; Radojković, A.; Žunić, M.; Dapčević, A.; Perać, S.; Branković, Z.; Branković, G. Evaluation of Stability and Functionality of BaCe_{1-x}In_xO_{3-δ} Electrolyte in a Wider Range of Indium Concentration. *J. Adv. Ceram.* **2022**, *11*, 443–453. [[CrossRef](#)]
48. Kane, N.; Luo, Z.; Zhou, Y.; Ding, Y.; Weidenbach, A.; Zhang, W.; Liu, M. Durable and High-Performance Thin-Film BHfYb-Coated BZCYb Bilayer Electrolytes for Proton-Conducting Reversible Solid Oxide Cells. *ACS Appl. Mater. Interfaces* **2023**, *15*, 32395–32403. [[CrossRef](#)] [[PubMed](#)]
49. Kim, Y.S.; Chang, W.; Jeong, H.J.; Kim, K.H.; Park, H.S.; Shim, J.H. High Performance of Protonic Ceramic Fuel Cells with 1-Mm-Thick Electrolytes Fabricated by Inkjet Printing. *Addit. Manuf.* **2023**, *71*, 103590. [[CrossRef](#)]

50. Bae, K.; Lee, S.; Jang, D.Y.; Kim, H.J.; Lee, H.; Shin, D.; Son, J.W.; Shim, J.H. High-Performance Protonic Ceramic Fuel Cells with Thin-Film Yttrium-Doped Barium Cerate-Zirconate Electrolytes on Compositionally Gradient Anodes. *ACS Appl. Mater. Interfaces* **2016**, *8*, 9097–9103. [[CrossRef](#)]
51. Kim, D.; Bae, K.T.; Kim, K.J.; Im, H.N.; Jang, S.; Oh, S.; Lee, S.W.; Shin, T.H.; Lee, K.T. High-Performance Protonic Ceramic Electrochemical Cells. *ACS Energy Lett.* **2022**, *7*, 2393–2400. [[CrossRef](#)]
52. Lee, K.R.; Tseng, C.J.; Jang, S.C.; Lin, J.C.; Wang, K.W.; Chang, J.K.; Chen, T.C.; Lee, S.W. Fabrication of Anode-Supported Thin BCZY Electrolyte Protonic Fuel Cells Using NiO Sintering Aid. *Int. J. Hydrogen Energy* **2019**, *44*, 23784–23792. [[CrossRef](#)]
53. Choi, S.M.; An, H.; Yoon, K.J.; Kim, B.K.; Lee, H.W.; Son, J.W.; Kim, H.; Shin, D.; Ji, H.I.; Lee, J.H. Electrochemical Analysis of High-Performance Protonic Ceramic Fuel Cells Based on a Columnar-Structured Thin Electrolyte. *Appl. Energy* **2019**, *233–234*, 29–36. [[CrossRef](#)]
54. Zhong, Z.; Li, Z.; Li, J.; Guo, X.; Hu, Q.; Feng, Y.; Sun, H. A Facile Method to Synthesize $\text{BaZr}_{0.1}\text{Ce}_{0.7}\text{Y}_{0.1}\text{Yb}_{0.1}\text{O}_{3-\delta}$ (BZCYYb) Nanopowders for the Application on Highly Conductive Proton-Conducting Electrolytes. *Int. J. Hydrogen Energy* **2022**, *47*, 40054–40066. [[CrossRef](#)]
55. Wang, M.; Wu, W.; Lin, Y.; Tang, W.; Gao, G.; Li, H.; Stewart, F.F.; Wang, L.; Yang, Y.; Ding, D. Improved Solid-State Reaction Method for Scaled-Up Synthesis of Ceramic Proton-Conducting Electrolyte Materials. *ACS Appl. Energy Mater.* **2023**, *6*, 8316–8326. [[CrossRef](#)]
56. Sari, S.N.; Nieroda, P.; Pasierb, P. The BaCeO_3 -Based Composite Protonic Conductors Prepared by Spark Plasma Sintering (SPS) and Free-Sintering Methods. *Int. J. Hydrogen Energy* **2023**, *48*, 29748–29758. [[CrossRef](#)]
57. Timurkutluk, C.; Timurkutluk, B.; Kaplan, Y. Experimental Optimization of the Fabrication Parameters for Anode-Supported Micro-Tubular Solid Oxide Fuel Cells. *Int. J. Hydrogen Energy* **2020**, *45*, 23294–23309. [[CrossRef](#)]
58. Ren, C.; Xu, P.; Zhang, Y.; Liu, T. Understanding the Polymer Binder Effect on the Microstructure and Performance of Micro-Tubular Solid Oxide Fuel Cells with Continuously Graded Pores Fabricated by the Phase Inversion Method. *Appl. Surf. Sci.* **2023**, *612*, 155928. [[CrossRef](#)]
59. Sun, H.; Zhang, S.; Li, C.; Rainwater, B.; Liu, Y.; Zhang, L.; Zhang, Y.; Li, C.; Liu, M. Atmospheric Plasma-Sprayed $\text{BaZr}_{0.1}\text{Ce}_{0.7}\text{Y}_{0.1}\text{Yb}_{0.1}\text{O}_{3-\delta}$ (BZCYYb) Electrolyte Membranes for Intermediate-Temperature Solid Oxide Fuel Cells. *Ceram. Int.* **2016**, *42*, 19231–19236. [[CrossRef](#)]
60. Xiao, Y.; Wang, M.; Bao, D.; Wang, Z.; Jin, F.; Wang, Y.; He, T. Performance of Fuel Electrode-Supported Tubular Protonic Ceramic Cells Prepared through Slip Casting and Dip-Coating Methods. *Catalysts* **2023**, *13*, 182. [[CrossRef](#)]
61. Hou, M.; Zhu, F.; Liu, Y.; Chen, Y. A High-Performance Fuel Electrode-Supported Tubular Protonic Ceramic Electrochemical Cell. *J. Eur. Ceram. Soc.* **2023**, *43*, 6200–6207. [[CrossRef](#)]
62. O'Neill, B.J.; Jackson, D.H.K.; Lee, J.; Canlas, C.; Stair, P.C.; Marshall, C.L.; Elam, J.W.; Kuech, T.F.; Dumesic, J.A.; Huber, G.W. Catalyst Design with Atomic Layer Deposition. *ACS Catal.* **2015**, *5*, 1804–1825. [[CrossRef](#)]
63. Kosaka, F.; Nakamura, T.; Otomo, J. Electrochemical Ammonia Synthesis Using Mixed Protonic-Electronic Conducting Cathodes with Exsolved Ru-Nanoparticles in Proton Conducting Electrolysis Cells. *J. Electrochem. Soc.* **2017**, *164*, F1323–F1330. [[CrossRef](#)]
64. Kim, J.; Jun, A.; Gwon, O.; Yoo, S.; Liu, M.; Shin, J.; Lim, T.H.; Kim, G. Hybrid-Solid Oxide Electrolysis Cell: A New Strategy for Efficient Hydrogen Production. *Nano Energy* **2018**, *44*, 121–126. [[CrossRef](#)]
65. Li, W.; Guan, B.; Ma, L.; Hu, S.; Zhang, N.; Liu, X. High Performing Triple-Conductive $\text{Pr}_2\text{NiO}_{4+\delta}$ Anode for Proton-Conducting Steam Solid Oxide Electrolysis Cell. *J. Mater. Chem. A* **2018**, *6*, 18057–18066. [[CrossRef](#)]
66. Ding, H.; Wu, W.; Jiang, C.; Ding, Y.; Bian, W.; Hu, B.; Singh, P.; Orme, C.J.; Wang, L.; Zhang, Y.; et al. Self-Sustainable Protonic Ceramic Electrochemical Cells Using a Triple Conducting Electrode for Hydrogen and Power Production. *Nat. Commun.* **2020**, *11*, 1907. [[CrossRef](#)]
67. Pei, K.; Zhou, Y.; Xu, K.; Zhang, H.; Ding, Y.; Zhao, B.; Yuan, W.; Sasaki, K.; Choi, Y.M.; Chen, Y.; et al. Surface Restructuring of a Perovskite-Type Air Electrode for Reversible Protonic Ceramic Electrochemical Cells. *Nat. Commun.* **2022**, *13*, 2207. [[CrossRef](#)] [[PubMed](#)]
68. He, F.; Zhou, Y.; Hu, T.; Xu, Y.; Hou, M.; Zhu, F.; Liu, D.; Zhang, H.; Xu, K.; Liu, M.; et al. An Efficient High-Entropy Perovskite-Type Air Electrode for Reversible Oxygen Reduction and Water Splitting in Protonic Ceramic Cells. *Adv. Mater.* **2023**, *35*, e2209469. [[CrossRef](#)]
69. Choi, S.; Davenport, T.C.; Haile, S.M. Protonic Ceramic Electrochemical Cells for Hydrogen Production and Electricity Generation: Exceptional Reversibility, Stability, and Demonstrated Faradaic Efficiency. *Energy Environ. Sci.* **2019**, *12*, 206–215. [[CrossRef](#)]
70. Saqib, M.; Choi, I.G.; Bae, H.; Park, K.; Shin, J.S.; Kim, Y.D.; Lee, J.I.; Jo, M.; Kim, Y.C.; Lee, K.S.; et al. Transition from Perovskite to Misfit-Layered Structure Materials: A Highly Oxygen Deficient and Stable Oxygen Electrode Catalyst. *Energy Environ. Sci.* **2021**, *14*, 2472–2484. [[CrossRef](#)]
71. Zhao, R.; Liu, C.; Zhang, X.; Zhu, X.; Wei, P.; Ji, L.; Guo, Y.; Gao, S.; Luo, Y.; Wang, Z.; et al. An Ultrasmall Ru₂P Nanoparticles-Reduced Graphene Oxide Hybrid: An Efficient Electrocatalyst for NH₃ Synthesis under Ambient Conditions. *J. Mater. Chem. A* **2020**, *8*, 77–81. [[CrossRef](#)]
72. Skúlason, E.; Bligaard, T.; Gudmundsdóttir, S.; Studt, F.; Rossmeisl, J.; Abild-Pedersen, F.; Vegge, T.; Jónsson, H.; Nørskov, J.K. A Theoretical Evaluation of Possible Transition Metal Electro-Catalysts for N₂ Reduction. *Phys. Chem. Chem. Phys.* **2012**, *14*, 1235–1245. [[CrossRef](#)]

73. Tao, H.; Choi, C.; Ding, L.X.; Jiang, Z.; Han, Z.; Jia, M.; Fan, Q.; Gao, Y.; Wang, H.; Robertson, A.W.; et al. Nitrogen Fixation by Ru Single-Atom Electrocatalytic Reduction. *Chem* **2019**, *5*, 204–214. [[CrossRef](#)]
74. Back, S.; Jung, Y. On the Mechanism of Electrochemical Ammonia Synthesis on the Ru Catalyst. *Phys. Chem. Chem. Phys.* **2016**, *18*, 9161–9166. [[CrossRef](#)]
75. Montoya, J.H.; Tsai, C.; Vojvodic, A.; Nørskov, J.K. The Challenge of Electrochemical Ammonia Synthesis: A New Perspective on the Role of Nitrogen Scaling Relations. *ChemSusChem* **2015**, *8*, 2180–2186. [[CrossRef](#)] [[PubMed](#)]
76. Mao, Y.J.; Wei, L.; Zhao, X.S.; Wei, Y.S.; Li, J.W.; Sheng, T.; Zhu, F.C.; Tian, N.; Zhou, Z.Y.; Sun, S.G. Excavated Cubic Platinum-Iridium Alloy Nanocrystals with High-Index Facets as Highly Efficient Electrocatalysts in N₂ Fixation to NH₃. *Chem. Commun.* **2019**, *55*, 9335–9338. [[CrossRef](#)] [[PubMed](#)]
77. Hao, R.; Sun, W.; Liu, Q.; Liu, X.; Chen, J.; Lv, X.; Li, W.; Liu, Y.p.; Shen, Z. Efficient Electrochemical Nitrogen Fixation over Isolated Pt Sites. *Small* **2020**, *16*, e2000015. [[CrossRef](#)] [[PubMed](#)]
78. Singh, A.R.; Rohr, B.A.; Schwalbe, J.A.; Cargnello, M.; Chan, K.; Jaramillo, T.F.; Chorkendorff, I.; Nørskov, J.K. Electrochemical Ammonia Synthesis—The Selectivity Challenge. *ACS Catal.* **2017**, *7*, 706–709. [[CrossRef](#)]
79. Xia, J.; Huang, K.; Yao, Z.; Zhang, B.; Li, S.; Chen, Z.; Wu, F.; Wu, J.; Huang, Y. Ternary Duplex FeCoNi Alloy Prepared by Cathode Plasma Electrolytic Deposition as a High-Efficient Electrocatalyst for Oxygen Evolution Reaction. *J. Alloy. Compd.* **2022**, *891*, 161934. [[CrossRef](#)]
80. Li, S.Y.; Nguyen, T.X.; Su, Y.H.; Lin, C.C.; Huang, Y.J.; Shen, Y.H.; Liu, C.P.; Ruan, J.J.; Chang, K.S.; Ting, J.M. Sputter-Deposited High Entropy Alloy Thin Film Electrocatalyst for Enhanced Oxygen Evolution Reaction Performance. *Small* **2022**, *18*, e2106127. [[CrossRef](#)]
81. Vøllestad, E.; Strandbakke, R.; Tarach, M.; Catalán-Martínez, D.; Fontaine, M.L.; Beeaff, D.; Clark, D.R.; Serra, J.M.; Norby, T. Mixed Proton and Electron Conducting Double Perovskite Anodes for Stable and Efficient Tubular Proton Ceramic Electrolysers. *Nat. Mater.* **2019**, *18*, 752–759. [[CrossRef](#)]
82. Hu, T.; Zhu, F.; Xia, J.; He, F.; Du, Z.; Zhou, Y.; Liu, Y.; Wang, H.; Chen, Y. In Situ Engineering of a Cobalt-Free Perovskite Air Electrode Enabling Efficient Reversible Oxygen Reduction/Evolution Reactions. *Adv. Funct. Mater.* **2023**, *33*, 2305567. [[CrossRef](#)]
83. Wan, Y.; Xing, Y.; Li, Y.; Huan, D.; Xia, C. Thermal Cycling Durability Improved by Doping Fluorine to PrBaCo₂O_{5+Δ} as Oxygen Reduction Reaction Electrocatalyst in Intermediate-Temperature Solid Oxide Fuel Cells. *J. Power Sources* **2018**, *402*, 363–372. [[CrossRef](#)]

Disclaimer/Publisher’s Note: The statements, opinions and data contained in all publications are solely those of the individual author(s) and contributor(s) and not of MDPI and/or the editor(s). MDPI and/or the editor(s) disclaim responsibility for any injury to people or property resulting from any ideas, methods, instructions or products referred to in the content.